Third Annual Report

on the

Mechanical Behavior of Polycrystalline Ceramics

Brittle Fracture of SiC - Si_3N_4 Materials

submitted to

The Lewis Research Center

Cleveland, Ohio

as part of

NASA Grant NGL 18-001-042

September 1, 1972

Submitted by:

Martin H. Leipold
Associate Professor of
Materials Science

Cawas M. Kapadia
Research Assistant

Anant H. Kelkar
Research Assistant

Introduction

This report represents a period of transition in this research program. The initial program had been concerned with the role of anion impurities on the behavior of a typical ceramic, magnesium oxide. The new effort is concentrated on the behavior of materials of considerable technological importance, silicon nitride and silicon carbide. The initial portion of this new research is directed toward our understanding the room temperature fracture behavior of various commercial materials. This report period also marks a change in the sponsoring agency from the National Aeronautics Space Administration, Washington, D. C., James J. Gangler, technical monitor, to the Lewis Research Center of NASA, Cleveland, Ohio, H. H. Probst, technical monitor.

Since the report will consider these two major activities it will be divided into two parts, Part 1 Oxide Research and Part 2 Nitride-Carbide Research. These two major activities will be further divided as necessary.

Part 1. Oxide Research

This phase of the research has emphasized the role of anion impurities on the fabrication and the behavior of magnesium oxide. The report is broken into subdivisions, each dealing with the individual phases of the research. For many of these phases, this report will represent a final report in that the work has reached a reasonable scientific conclusion and no additional avenues of investigation are anticipated. In other cases, primary questions remain unanswered and some studies will continue, although at continually decreasing emphasis as the existing problems are resolved. No new phases of study will be introduced in this portion of the research.

Section I. Fabrication

The effort here was designed to determine the effect of anion impurities on the hot pressing behavior of MgO. Since it was necessary to fabricate specimens prior to study of their other properties, this activity received heavy emphasis during the early stage of the research. The results are reported in earlier annual reports.[1,2] During this last year the only effort has been directed toward publication of these results. A publication has been submitted to the American Ceramic Society.

Section II. Grain Boundary Microhardness

Extensive additional results are being obtained to confirm the earlier reported results.[2] Although the experimental results are nearly all completed, the results are not in a form for presentation. These results will be compiled and analyzed in the near future. No additional experimental work is anticipated.

Section III. Grain Growth

Further work on grain growth studies in MgO in presence of anion impurities has been carried out. Anneals have been completed at 1300°C and 1500°C and annealing times ranged from 1 hr. to 200 hrs. Details of the experimental procedures and techniques have been given in earlier annual reports.[1,2] The anion dopants added initially were at a concentration of 3 at.%

but considerably less were retained in the as-pressed samples. As reported in the Second Annual Report[2], these dopants as a group did not inhibit grain growth in MgO and at levels of 3 at.%, no appreciable retarding influence of dopants was observed. Hence, it was decided to determine whether a higher initial concentration of the dopant would influence growth kinetics.

Among the dopants, the quantities of Cl^- and $S^=$ retained were particularly lower and hence specimens with higher initial concentration of sulphur (6 at.%) were hot pressed to be used subsequently for grain growth studies. These as-pressed samples, when analyzed, showed about the same level of sulphur retained as the previous ones. This could be accounted for by the high volatility of the species. Specimens with higher concentration of Cl^- have not been prepared to date.

Many of the anion containing specimens were of lower density (See Annual Reports I and II). Consequently, some further studies of grain growth in doped MgO specimens with higher as pressed densities (> 96% theoretical) are being carried out presently. The specimens studied previously were hot-pressed to intermediate stage densities and hence contained open porosity. This led to a possibility of further loss of the volatile dopant during the grain growth anneals carried out in open atmosphere giving a gradual variation in their concentration for a given specimen at different anneal periods. Also, if concentrations reached negligible levels after fairly long anneal time, then the influence of these anions on grain growth kinetics cannot be established.

In specimens with a higher as pressed densities (final stage), the possibility of further loss of these volatile species during grain growth anneals is considerably lessened and hence the studies of any effect of anions on kinetics would be more apparent. A summary of these runs is given in Table I. Previously OH^- doped MgO was studied only at 1500°C. Data is now obtained for temperature of 1300°C as well.

The data are analyzed differently than previously. The grain growth kinetics is readily given by the expression

$$D_t^n - D_o^n = kt \qquad (1)$$

where

D_o = initial grain size at anneal time = 0

D_t = average linear intercept grain size at anneal time = t

k = rate constant

n = grain growth exponent

The object of our studies has been to determine the effect of the different anions on the exponent n, and the constant k (which gives the activation energy).

Previous results[2] indicated that, for our impure porous materials, grain sizes were comparable to other workers using high purity high density material[3] after the same annealing time. Thus, difference in D_o and/or k is suggested since the grain growth rate exponent was larger (~ 3 compared to 2), which would indicate a lower rate of growth.

Previously the initial grain size (D_o) had been altogether neglected (which is reasonable for large anneal periods) to give the expression

$$D_t^n = kt \qquad (2)$$

A plot of log D_t against log t would give a slope which is the reciprocal of the exponent n.

In the present work, D_o is taken into account and the expression (1) is used. As the as-pressed grain size ($\lesssim 1\mu$) is less than optical resolution it was decided to take D_o as the grain size after a 10 min. anneal. This period was deducted from subsequent annealing times.

A computer program was developed to plot log $\left(D_t^n - D_o^n\right)$ against log t with n ranging from 2 (as predicted for ultra high purity and very dense specimens) to higher values as expected in materials containing impurities except at very high temperatures. The value of n which gives a slope of unity would define the exponent n for the particular set of data. Most workers observe a value of n ~ 3 or greater. This is because of limiting grain growth brought about by the interaction of grain boundaries with inclusions.[4,5]

A linear least square plot for specimen #134 (sulfur doped MgO) annealed at 1300°C is given in Fig. 1. Value of n = 2.93 gave a slope of 1.0005. Similar studies for other specimens are underway presently.

In addition to these studies of the functional relationship of these grain growth kinetics, effort has been directed to determining any effects on the microstructure. This includes the development of pores, precipitates, and second phases. There is also a growing evidence that impurity segregation at grain boundaries influences final stage sintering of ceramic oxides and induces grain boundary hardening.[6,7] This justifies the growing concern for determining the composition of grain boundaries in terms of separating the influence of impurities inherently present in the as-received material and the specific dopants that have been added. Only then it would be possible to decide on the effect of these dopants on processes like densification and grain growth.

Techniques which could give us answers are optical microscopy, X-ray analysis, electron microprobe analysis and electron microscopy. The optical microscopy could at the best give some idea about quantity and distribution of second phases but are limited to resolution of about 1μ. If the precipitate was coherent to the matrix, it would have a region of strained matrix around it (difference in size effect). This strained region would give birefringence in an otherwise optically isotropic material like MgO and hence would show up in plane polarized light. This effect would not be observed if the inclusions were pores filled with some volatile species since gas pressure would be insufficient to produce significant lattice strain. Such studies were undertaken, and though id did lead to distinguishing between a pore and a solid second phase, it did not lead to determining of solid phase itself.

X-ray diffraction would permit determination of the nature of the precipitates by revealing additional diffraction peaks characteristic of the compound present. However, here the small quantity of such compounds, if any, suggests that X-ray analysis would not seem very helpful. Further, it would give us a bulk analysis rather than the spatial distribution (grain boundary or in the lattice) that is of concern here.

Electron microprobe analysis would seem like very fruitful approach in determining both the nature of the inclusions and their distribution. Though work has been done in study of cationic impurity segregation along the grain boundary in MgO[8], no systemmatic investigations of anionic impurities or their compounds with Mg have been made. Among the anions studied here, the microprobe may have a low sensitivity for F^- because of its low atomic weight and no sensitivity for OH^-. Further, equipment is not conveniently available.

Some work on transmission electron microscopy has been attempted. Surface replicas were made using chromium as a shadowing agent. However, little information was gained on the nature of the grain boundaries. A typical electron micrograph of a fluorine doped specimen shows tiny platelets which could be precipitate particles oriented in certain directions. See Fig. 2.

More extensive work has been done on the scanning electron microscope (SEM). This method is convenient because it does not require any elaborate sample preparation. The samples were polished by conventional techniques[2] and etched very lightly in 85% H_3PO_4 (2 parts) and 70% H_2SO_4 (one part) or were prepared by fracturing. The samples were mounted on the holder with Duco cement. Electrical continuity between oxide sample surface and the metallic holder was maintained by a thin streak of conductive silver paint. The surface of the specimen was coated in a vacuum evaporator with a Au-Pd alloy to give a good electrical conductivity. Scanning electron micrographs of two different regions of a fracture surface of sulphur doped samples are shown in Fig. 3. These are as-pressed samples with grain size of about

1μ. We clearly see inclusions of order of 10μ size which have a different texture than the matrix. The inclusions seem to be separated from the matrix. This might be due to difference in volume expansion coefficient of inclusions and the MgO lattice which generated thermal stress on cooling after hot pressing. These cracks may also have developed during fracture as a result of a difference in hardness. Also, the precipitate regions appeared lighter than the background. It is not known whether this is due to precipitate phase which is of higher atomic weight than the MgO matrix or due to an accumulation of a static charge on the particle which has lost electrical continuity with rest of the sample surface.

A polished and etched surface for a sulphur doped specimen which has been reheated for 48 hours at 1500°C is shown in Fig. 4. Again the appearance of a lighter phase at one of the triple points and along some grain boundaries might suggest a second phase of higher atomic weight, probably a calcium silicate from the impurities present initially in the as-received material. The darker phases at the other triple points seem to be identical in atomic weight with phases found elsewhere within the grains and at grain boundary.

Although these darker phases seem to be just coalesced porosity, a closer examination reveals that there is some solid phase present. In fact, one can even see some tiny pores in these solid phases as shown by arrow Fig. 4b.

It might be possible to infer something about the nature of the second phase from their morphology. The contact angle (θ) between the second phase (β) and the matrix (α) depends on the ratio of grain boundary energy ($\gamma_{\alpha\alpha}$) to interphase energy ($\gamma_{\alpha\beta}$). The fact that this angle is less than 120° suggest that $\gamma_{\alpha\alpha} > \gamma_{\alpha\beta}$ and that the second phase is not just a pore filled with "MgO vapor" since in that case, $\gamma_{\alpha\beta} > \gamma_{\alpha\alpha}$. At the first triple point we definitely see a darker phase which wets the lighter phase (major phase at triple point) and gives a rather small contact angle for the interface with MgO grain. This indicates a possible phase consisting of a species which is of a lower atomic weight and also a higher polarizability which gives the low value for the interface energy. Measurement of this contact angle would permit determination of the interphase surface energy between MgO and second phase. If data regarding such energies between MgO and other compounds were available, it would be possible to determine the compound. Unfortunately such data is not readily available and there appears to be no consistency in the magnitude of the various contact angles.

Summarizing the results of the determination of the microstructure, optical studies did not reveal second phase structure. X-ray analysis was not attempted because of very small quantities of second phases expected. Microprobe studies were not made, as easy access to a unit was not available. Electron microscope studies were performed, but the scanning electron microscope was especially useful and gave qualitative information which could be used for more detailed studies.

Some work will continue to determine the location of the anions in this compact, since complete explanation of the many portions of the research can be made only with such knowledge.

<u>Section IV. Diffusion</u>

The diffusion experiments in this research were to determine whether an cation vacancy structure existed at the grain boundaries in MgO in the presence of these anions. It has been suggested that enhanced diffusion at grain boundaries in MgO results largely from the existence of an impurity network.[9] If such a model is correct, then the effect should be noted when a vacancy structure exists on one lattice as a result of charge imbalancing impurities on the other. The specific approach here was to study the diffusion of a cation (nickel) into polycrystalline MgO which had been doped with potential charge imbalancing anions. The vacancies then would occur on the cation lattice. The diffusion anneals were made in large grained MgO in the region of predominately grain boundary diffusion (1200 °C). The fabrication and reheat parameters for these specimens are given in Tables 2 and 3. The diffusion anneals were conducted with the dense MgO specimen surrounded by a NiO powder compact. The diffusion profiles on an interior section were determined in an electron beam microprobe* at 20 KV and 0.05μ amp beam current. A defocused beam (10μ diam.) was used in the manner shown in Figure 5. Total counts for Ni Kα and Mg Kα were determined as a function of distance with integrated beam current being constant for each distance step. Sensitivities and backgrounds for Mg were determined by the dense MgO interior and for Ni by the porous NiO around the specimen as well as separate dense NiO specimens.

The atomic fraction Ni was calculated and plotted as a function of concentration. Such a plot is expected to be linear according to the basic equation for grain boundary diffusion with a constant source of diffusing atoms $C(0,0) = C(0,t) = k$. For these conditions

$$C(x,t) = K\left(\frac{Dt}{\delta^2}\right)^{\frac{1}{2}} \exp - \left(\frac{4\ D}{\pi\,(\delta D')^2\ t}\right)^{\frac{1}{4}} \quad x$$

where C is the concentration at

x distance

t time

D is the lattice diffusion constant

D′ is the grain boundary diffusion constant

δ is the grain boundary width

K is a constant

Under conditions of constant D, t, δ,

$$\ln C = K_1 - \left(\frac{4}{\pi}\frac{D}{(\delta D')^2 t}\right)^{\frac{1}{4}} \quad x$$

Hence, a plot of $\ln C$ is linear with x and the slope defines ($\delta D'$) since D and t are known. Considerable debate is underway concerning the validity of

---

*Applied Research Lab., Glendale, Calif., Analyst Model courtesy of G. Asgar, Professor of Dental Materials, College of Dentistry, University of Michigan, Ann Arbor, Michigan.

this analysis and the possibility of separating δ and D'. This approach will be used here since our data do fit the ℓn C vs x form and comparative literature data uses this form.

The results for each of the profiles are shown in Figures 6-9 and the linear form in the region of grain boundary diffusion is quite good. A composite plot is given in Figure 10 with the slopes and diffusivities in Table 4. These data indicate no effect of the various dopants on the grain boundary.

Comparison of these results with the only quantitative data in literature is shown in Figure 11. The scatter in the available data is quite large and so precise conclusions cannot be drawn. However, if a least squares determination of all data is used, the noted 1.71 eV is obtained, with 1 and 2 eV slopes given for comparison. Since the diffusion of Ni^{+2} into a single crystal MgO has an activation energy of 2.1 eV and activation energy for grain boundary diffusion would be expected to be between 0.5 and 1.0 of this, the value is in a reasonable range.

Additional anneals (See Table 5) have been made at temperatures of 1000-1400°C and profiles will be obtained to define the activation energy for each anion. This will mark the conclusion of this phase of the oxide research.

Section V. Chemical Analysis

The analytical studies in this research served to properly characterize the composition of the materials in use. However, in some cases, e.g., the existence of OD^- in MgO, some research was necessary and has been reported earlier[1,2] During this period, only routine documentation studies have been conducted and results are included where applicable. Only minor amounts of such work are anticipated in the future to finally characterize other results.

Part 2. Nitride-Carbide Research

Silicon nitride and silicon carbide are very useful structural materials for high temperature application such as in gas-turbine engines because of their properties such as very high fracture energy, low thermal expansion and good thermal conductivity. (See Table 6.) Also they have good inherent corrosion and abrasion resistance to the gaseous environment and have high temperature stability. To improve the fracture toughness of these materials in order to make them more reliable as structural materials, their fracture mechanisms should be clearly understood. This is plausible since fracture is, at least in part, microstructure controlled, while the others are much less so. Here an attempt is made to understand the various mechanisms taking place during the fracture of silicon nitride under controlled conditions and to correlate the fracture toughness to the microstructure.

Even though the mechanisms taking place during the fracture of Si_3N_4 and SiC are not established, many research workers have done investigations in this field and hence a survey was conducted to judge the present status of knowledge of crack propagation in SiC and Si_3N_4. The results of this survey are given below:

1. It is found by Evans and Davidge[10] that fracture in reaction sintered Si_3N_4 occurs by the extension of inherent flaws, the largest pore in this case, in a brittle manner.
2. In hot pressed Si_3N_4, the inherent flaws are thought to be associated with unidentified structural features which were much larger than the average grain size.[11] The fracture may be taking place by extension of these flaws.
3. The fracture mechanism in Si C is unresolved.
4. In case of Si C, generation and motion of dislocation occurs during a crack propagation even at room temperature[12] but only on a very limited scale. The dislocations are identified as having Burgers vector $b = a/2 <110>$ and the operating slip plane to be $\{111\}$.

5. No dislocation motion has been observed during crack propagation in Si_3N_4.

6. Fracture surfaces of Si C show features like cleavage steps and river patterns which are typical of crystalline or glassy materials[13] No explanation has been provided for the result.

7. Evans and Davidge[14] observed increase in the value of fracture energy with increase in density of reaction sintered Si_3N_4.

8. The fracture stress in case of reaction sintered Si_3N_4 is relatively independent of temperature up to 1700°C.

It is not known whether the same result exists for hot pressed Si_3N_4

9. Grain morphology plays an important role in the resistance offered to the crack propagation. Lange and Terwillinger[15] observed that fracture energy of hot pressed Si_3N_4 when starting with α-phase material and with elongated final grains was four times the value when starting with β-phase material and equiaxed grains.

Section I. Development of the Fracture Toughness Testing Technique

To evaluate and compare the capacity of a material which does not deform plastically, fracture toughness is considered to be a very useful parameter.

The fracture energy indicates the amount of energy absorbed by a unit area of fracture surface at the start of crack propagation. In the conventional fracture toughness testing, the fracture energy (γ) is determined by measuring the force required to propagate a sharp crack previously introduced in the specimen. For ceramic materials, usually double cantilever beam (DCB) configuration of specimen is used. Here γ is a function of both load and the crack length. Therefore, as the crack propagates, the lever arm increases and the load required for constant stress intensity factor at the crack tip decreases (assuming constant γ). Since reducing the load at the required rate is impractical, the crack propagation takes place under increasing load and normally the crack velocity increases. This type of testing is limited for studying the fracture mechanisms, since the control of velocity is lacking.

In this part of the program, a new method of measuring fracture toughness, with a modified double cantilever beam configuration of specimen, is being utilized. This technique, applying a constant moment beam (CMB) is designated to keep the velocity constant and jigs were designed to use this technique. The crack velocity can be controlled and measured with this technique and would appear to be very useful for fracture study. It will be described in greater detail later in this report. During these investigations, conventional DCB will also be used for comparison.

As Si_3N_4 is a brittle ceramic material, with little or no plastic deformation occurring during the fracture, other available brittle materials like glass and alumina are being used to develop the conventional and modified methods of fracture toughness testing in the laboratory. The results of these two methods will then be compared.

A. <u>Conventional fracture toughness test (DCB)</u>

The fracture energy γ using a double cantilever configuration is given by[17, 18]

$$\gamma = [\, 6F^2 L^2/EW^2 t^3 \,]\,[\, 1 + 1.32 \frac{t}{L} + 0.542(\frac{t}{L})^2 \,] \qquad (3)$$

where (See Fig. 16b) .

F = the force required to cause the fracture

L = the length of the pre-existing crack

E = Elastic modulus of the material

W = Thickness of the specimen

t = Perpendicular distance between the crack and edge of specimen.

Rectangular specimens 1" x 0.5" were prepared by diamond cutting of microscope slides. A slot of ~ 0.35" length was machined in the rectangular specimen by means of a diamond wheel. The wax, used for sticking many specimens together for the ease of machining, was removed with acetone, and the specimen surfaces were cleaned and dried. The specimen was observed under microscope and it was verified that the specimen, initially, was free from cracks.

A sharp crack at the tip of the slot was introduced by thermal shock. The specimen was heated to about 500°F for 15 minutes and then a very tiny drop of water was put at the tip of the slot by means of a thin cu-wire while the specimen was on the heater. Attempt was made to produce the crack in the direction of the slot or parallel to the edge of the specimen and right in the center of the tip of the slot as it is shown in Fig. 12. But the attempt was not successful and general form of the crack obtained was as shown in Fig. 13a. The crack was observed under the microscope and the dimensions L, t were measured by using the microscope scale.

Thin Cu wires which could withstand a force of 10 pounds without yielding, were fastened for the application of the force on either side of the slot by means of epoxy. This specimen (Fig. 13b) was then tested in Instron for fracture toughness. The tensile load was applied with the holder moving at the rate of 0.02"/min. The force required to fracture the specimen was recorded.

The values of γ for glass obtained here (See Table 7) are comparable to γ as observed by Wiederhorn[19] (3900 ergs/cm^2). The later value will correspond to the fracture when the initial sharp crack is in the direction of the groove so that its path of propagation is parallel to the edge of the specimen.

The deviation in values of γ obtained here from those obtained by Wiederhorn must be mainly due to the variation in the path of crack propagation. Here the crack always propagated in the direction of the initial sharp crack so that the resulting fracture was as shown in Fig. 13c.

In this type of crack propagation the formula used for γ should be modified but such modification is not available.

The low value of γ in specimen No. 6N might be because the initial sharp crack appeared larger than normal so that less force was required to fracture the specimen.

New DCB specimens of glass slides were prepared as before, but this time, grooves were cut (Fig. 14) with a diamond wheel on either side of the specimen, along the direction of the slot to guide the path of crack propagation.

The modified formula (with the changes in specimen geometry) for fracture energy is as follows:

When the fracture is along the grove:

$$\gamma = \left[\frac{6F^2 L^2}{E\ W\ bt^3}\right]\left[1 + 1.32\ \frac{t}{L} + 0.542\left(\frac{t}{L}\right)^2\right] \tag{4}$$

where b = Web thickness

and the other terms as defined in Eqn. 3.

When the fracture leaves the groove, b = W and this equation reverts to the previously used Eqn. (3).

The values obtained for the specimens which fractured along the groove (in the direction normal to that of applied tensile stress) were fairly constant. When the fracture left the groove, values varied greatly.

Additional preliminary information was obtained by DCB measurements of fracture energy of alumina. Rectangular plates 1" x 0.5" of alumina were prepared by diamond cutting. A slot of ~ 0.35" length was machined in the rectangular plate and grooves were also cut on either side of the plate by means of a diamond wheel. The plate was observed under microscope to verify that it was initially free from cracks.

A sharp crack could not be introduced in this specimen by means of thermal shock (putting a tiny drop of water on a hot specimen). This must be attributed to the high fracture strength of alumina. Wedge technique was found to be successful. The specimens were clamped at the bottom and a wedge was slowly forced into the slot (Fig. 15). A sharp crack could be observed under the microscope. Dye penetrant† (red in color) was used to make the crack clearly visible and the crack length was measured.

To carry out the fracture toughness test, using a tensile stress with the Instron, wires were attached to the specimen by means of epoxy. When this specimen was connected to the Instron, the specimen failed as soon as the stress was applied. Apparently the small sharp crack had penetrated up to the full length of the specimen while attaching wires to the specimen by means of epoxy. The method of attaching wires to the specimen must be modified and drilling holes in the specimen should be a better method. The sharp crack should be introduced after the holes are drilled. This work is continuing.

B. Constant Moment Beam (CMB)

The previously mentioned fracture technique[16] employs a moment independent of the crack length and will be referred to as the constant moment beam (CMB). Energy is introduced at the crack tip by the application of a load to the arms attached to the specimen. (See Fig. 16a). Here the strain energy release rate is independent of crack length and is given by

$$G = \frac{M^2}{E\,I\,t} \tag{5}$$

where M = the moment placed on one arm

I = the moment of inertia of one side of the specimen about its longitudinal axis

E = the elastic modulus of the material

t = the thickness of the specimen at the center groove used to guide the crack.

For a homogeneous material, G will be constant and hence for a particular specimen M would be constant when the load (F) is kept constant.

† Spot check by Magnaflux Co.

Because crack length is proportional to deflection, crack velocity $\frac{da}{dT}$ can be obtained from

$$\frac{da}{dT} = \frac{EI}{ML} \frac{d\,\delta}{d\,T} \tag{6}$$

where L is the distance from the point of measurement to the fulcrum

δ is the deflection of the arm

T is the time.

The final design of the jig designed for this technique is shown in Fig. 17. Load is applied to Parts IV by the Instron and will be transmitted to Parts III, so that Part II will rotate about point A. The specimen is held between Parts I and II by a rigid three line grip, which transmits a torque to the specimen arms M and the arms M rotate. The deflection of the jig is measured by the movement of the tip of the transducer, fixed to Part V, and is recorded on a moving chart to determine the crack velocity.

The anticipated load in the unit during test was determined in the following manner. A load F is applied by the instron on Parts IV of the jig and load $\frac{F}{2}$ will be transferred to each of Parts III at points B. The resultant moment on the specimen arm will be $= \frac{F}{2} \times L$ where L is the distance between the point B and the fulcrum A. (More than one hole is drilled at distance 0.5'' apart on Parts II and VI to fix Part III, so that length L can be changed, if desired.)

In the equation (5) and with

$G = 120,000\ \text{erg/cm}^2$ for Si_3N_4

$E = 45 \times 10^6$ psi

$I = 0.318$ gm-cm^2 for a specimen

H = 3 cm
w = .23 cm
t = .114 cm
h = .7 cm

(See Fig. 16b)

for a value of arm L of the moment M = 2.54 cm, the expected load $\frac{F}{2}$ is about 50 kg and the corresponding total load F by the Instron is 100kg. The test jig is made of strainless steel and was designed to easily bear this load without deforming permanently. The unit has been constructed and its performance is being evaluated at present.

The specimen geometry used for this technique is shown in Fig. 16b. This specimen configuration and this method of transmission of moment eliminated the problem of drilling holes in Si_3N_4 specimen. Previous attempts to drill holes in Si_3N_4 pieces with diamond drills were somewhat unsuccessful. About 30 minutes was required to drill a hole of 0.125" dia., 2 mm. deep in a piece of reaction sintered Si_3N_4 (which has lower density than hot pressed Si_3N_4). Drift of the hole was also encountered. Ultrasonic drilling used successfully by others is not available.

C. Production of Microcrack

In either fracture toughness test, the specimen is fractured by the extension of a microcrack of known length produced in the specimen. The method of producing the required microcrack is of some importance in the test. Thermal shock or wedging are normally used but in a material as strong as silicon nitride, it is thought that production of the microcrack should be easier and more controllable applying load with the testing machine. The specimen without any crack is held in the jig and the middle is tightly held in a clamp at a distance of 1/16" from the tip of the notch of the specimen. Tensile load is slowly applied to the specimen and at some load, a crack will be produced at the notch and will propagate until it is arrested by the compression stress field produced by the clamp on the specimen.

Section II. Microstructure Examination

The fracture toughness of a ceramic material depends on the microstructural features like grain size, grain morphology, the presence of a second phase and porosity. The effect of these variables is not clearly understood in case of silicon nitride and in this program, efforts will be made to correlate the values of fracture toughness obtained to the available microstructural variable in Si_3N_4. Because Si_3N_4 has not received extensive study and because it is difficult to process, polishing and etching techniques are being developed to obtain a convenient method of examining the microstructure of Si_3N_4.

Polishing Technique

First, the specimen was mounted on a plastic mould. The mounted specimen was then polished on successively finer diamond wheels from 100 mesh to 6 micron. About 2-4 minutes per wheel was used. Then the specimen was polished on a wet cloth with 0.3 micron alumina powder suspension in water for 15 minutes and then with 0.05 micron alumina for 10-12 hours in a vibratory polisher.

The final polished surface is shown in Fig. 18. The photograph shows the presence of bright, spherical particles of size 0.5-1μ. Some dark grains of Si_3N_4 are also seen as a result of relief polishing.

Etching Techniques

Si_3N_4 is a very hard and chemically inert material and its etching presents some difficulties. All the following etching techniques suggested in the literature were tried with no success to the present and a suitable method will be developed.

Boiling phosphoric acid at 200°C with a concentration of 94.5% H_3PO_4 is reported to have an etching rate of 200A°/min.[20] Examination of the surfaces of specimen under scanning electron microscope after several hours of etching in phosphoric acid showed no etching. Longer etching times (several days) were then used and a change in color of the specimen was noted from black to white. An SiO_2 coating on the surface of the specimen is believed to be the reason for this change and the specimen was therefore placed in hydrofloric acid for 1/2 hour to remove SiO_2. These specimens were then observed under SEM with scanning electron microscopy.

Figure 19 shows the structures observed. The plate-like structure in Fig. 19 is believed to be SiO_2.

The network of bright lines in Figure 20 are too thick to be the grain boundaries. Some structure is evident which may be grains but are not clearly distinguished from one another. The etching might have been insufficient, however, since the technique is already time consuming, it will be further pursued if other methods do not work.

A mixture of K_2CO_3 and NaF (8:1 proportion by weight was heated in a porcelain crucible to 740°C. Demounted polished specimen was put in the molten salt bath at 740°C and kept there for 3-4 min. then the specimen was removed from the bath and immediately put in conc. HCl. This was done to dissolve the solidified salt mixture, adhering to the specimen.

The structure showed fiborous, bright material clinging to the surface of the specimen and it covered the surface almost completely and the actual surface of the specimen could not be seen. Any further treatment with conc. HCl or with HF could not change the nature of the surface. The specimen was repolished with 0.05μ Alumina for 10-15 sec. to remove this material but was unsuccessful. It was then repolished with 0.3 Alumina which removed the surface coating but no grain structure was observed. The surface was the same as the polished specimen.

Other etching techniques are being evaluated such as boiling mixture of 30 CC HF, 25 CC H_2O_2 and 5 CC HNO_3. These techniques will also be further pursued.

References

1. M. H. Leipold, et al., "Role of Anions in Mechanical Failure," First Annual Report, U. of Ky. TR 25-70 Met. 12, June 1970.

2. M. H. Leipold, et al., "Role of Anions in Mechanical Failure," Second Annual Report, U. of Ky. TR 42-71 Met. 4, Aug. 1971.

3. R. M. Spriggs, L. A. Brissette, and T. Vasilos, "Grain Growth in Fully Dense MgO, J. Amer. Cer. Soc., 47 (8), (1964) 417.

4. C. S. Smith, Trans. AIME, 175, (1948) 15.

5. J. W. Cahn, "Impurity Drag in Grain Boundary Motion," Acta Metallurgica, 10, (1962) 789-798.

6. P. Jorgenson and J. Westbrook, "Role of Solute Segregation at Grain Boundaries During Final-Stage Sintering of Aluminum," Jn. of Am. Cer. Soc., 47, (7), (1964) 332-338.

7. H. Sjodahl and J. Westbrook, "Solute Induced Grain Boundary Hardening and the Sintering of BeO," ibid 48, 9, (1965) 478-480.

8. M. H. Leipold and T. H. Neilsen, "Impurity Distribution in MgO," ibid 49 (9), (1966) 498.

9. B. J. Weunsch and T. Vasilos, ibid 47 (2) Feb. 1964.

10. A. G. Evans, R. W. Davidge, J. Material Sci. 5 (1970) 314-325.

11. R. J. Lumby, R. F. Coe, Proc. Brit. Ceram. Soc. 15 (1970) 91.

12. R. Stevens; J. Mater. Sci. 5 (1970) 474.

13. MRI Report, Project No. 3270C, Contract No. N00019-69-C-0161.

14. R. W. Davidge and A. G. Evans, Mater. Sci. Eng. 4 (1970) 281-298.

15. F. F. Lange and G. R. Terwillinger, "Fabrication and Preparation of Si-compounds," Contract No. N00019-17-C-0107 Nar. Air Sys. Com. Dept. of Navy.

16. S. W. Freiman, et al., "Crack Propagation in Ceramics," Report of NRL Progress, Feb. 1972, p. 36.

17. J. E. Srawley and B. Gross, "Stress Intensity Factors for Crackline-Loaded Edge Crack Specimens," Mat. Res. Stand. 7 (4) (1967) 155-162.

18. S. M. Wiederhorn, A. M. Sharp, and R. L. Moses, "Cricical Analysis of the Theory of the Double Cantilever Method of Measuring Fracture-Surface Energies," J. Appl. Phys. 39 (3) (1968) 1569-1572.

19. W. Van Gedder, and V. E. Hanser, J. Electrochem. Soc., 114 (8), (1967) 869-872.

20. S. M. Wiederhorn, "Mechanical and Thermal Properties of Ceramics," J. B. Watchman, Ed., NBS spec. Pub. 303, May 1969, pp. 217-241.

Table 1

Characteristics of Specimens Used in Grain Growth Studies

Specimen No.	Dopant At. %	Hot Pressing Conditions Pressing Temp(°C)	Atmos.	As-pressed density gm.	As-pressed analysis At. %
134	6 $S^{=}$	1000	Argon	3.55	0.036 S
115	3 Cl^{-}	1100	Vacuum	3.56	0.057 Cl
114	3 F^{-}	1100	Vacuum	3.56	0.421 F
120	3 OH^{-}	1100	Vacuum	3.52	N.A.*
130	Undoped	1000	Argon	3.52	-
132	Undoped	1000	Argon	3.56	-

* N.A. Not available.

Table 2. Composition and fabrication parameters for Specimens for annion-doped MgO diffusion anneals.

Spec	Initial Dopant at%	Max Temp °C	Max Pressure PSI	Time At Temp Hr	Atm	Pressed Density Gm/Cm^3	Final Dopant at%
30	0.58%S	960	20,000	2	Vac.	3.55	0.03
110	3.0%F	1100	15,000	2	Vac.	3.53	(0.90)
115	3.0%Cl	1100	15,000	10	Vac	3.56	0.06

Table 3. Grain growth and diffusion anneal parameters for anion-doped MgO.

	Grain Growth				Diffusion Anneal	
Spec #	Temp. °C	Time Hr	Final Comp at%	Final Grain size μ	Temp °C	Time Hr
30	1500	60	(.04)	60	1200	170
110	1300	200	(.02)	64	1200	170
115(1)	1300	67	(.03)	140	1200	170
(2)	1300	214	(.03)	220	1200	170

Table 4

Grain Boundary Diffusion Constant ($\delta D'$)
at 1200°C for Ni in Anion-Doped MgO

Sample	Dopant	Slope	$\frac{(\delta D')^2}{D}$	$\delta D'$
		μ^{-1}	cm^4-sec^{-1}	$cm^3\ sec^{-1}$
30	$S^{=}$	.035	0.49×10^{-15}	2.4×10^{-14}
110	F^-	.0272	1.35×10^{-15}	4.01×10^{-14}
115(1)	Cl^-	.0270	1.39×10^{-15}	4.08×10^{-14}
115(2)	Cl^-	.0254	1.78×10^{-15}	4.62×10^{-14}

$\delta D'$ based on $D = 1.2 \times 10^{-12} cm^2 \text{-} sec^{-1}$ @ 1200°C

Wuensch & Vasilos

Table 5

Diffusion Anneal Specimens Completed and Awaiting Microprobe Analysis

Sample #	Dopant
30	0.58% S (as pressed)
110	F
115	Cl (0.057% as pressed)
120	2% OH
132	Undoped

Table 6

Typical Properties of Silicon Nitride and Silicon Carbide

Property	Value Silicon Nitride	Silicon Carbide
Fracture energy ergs/cm^2	60,000	30,000
Coeff of thermal expansion /°C	2.75×10^{-6}	4×10^{-6}
Thermal Conductivity Btu/hr ft^2/in/°F	116	150
Max. Use Temperature °C	1650	2,000

TABLE 7

Fracture Energy for Glass Microscope Slides

$E = 8.06 \times 10^{11}$ dynes/cm^2 = 11.7×10^6 psi.

Specimen geometry: DCB (no side grooves)

Specimen No.	L inch	Mean t inch	B inch	W inch	F lbs.	γ_f Ergs/cm^2
1N	0.353	0.216	-	0.0394	1.7	4170
2N	0.374	0.193	-	"	1.36	3803
3N	0.372	0.216	-	"	1.39	3005
4N	0.36	0.222	-	"	1.525	3499
5N	0.35	0.217	-	"	> 1.84	> 4847
6N	0.37	0.212	-	"	0.98	1548
7N	0.33	0.217	-	"	2.3	6970

Specimen geometry: DCB (with side grooves)

Specimen No.	L inch	Mean t inch	B inch	W inch	F lbs.	γ_f Ergs/cm^2	Type of Fracture
1G	0.41	0.253	0.02	0.0394	1.4	4260	Along the groove
2G	0.68	0.238	0.017	"	0.64	4440	"
3G	0.35	0.253	0.022	"	1.34	3430	"
4G	0.39	0.237	0.026	"	1.6	4800	"
5G	0.42	0.253	0.029	"	1.3		Out of the groove
6G	0.63	0.23	0.030	"	1.36	5698	"
7G	0.56	0.274	0.028	"	> 1.7	4546	"
8G	0.37	0.23	0.029	"	1.06	1479	"

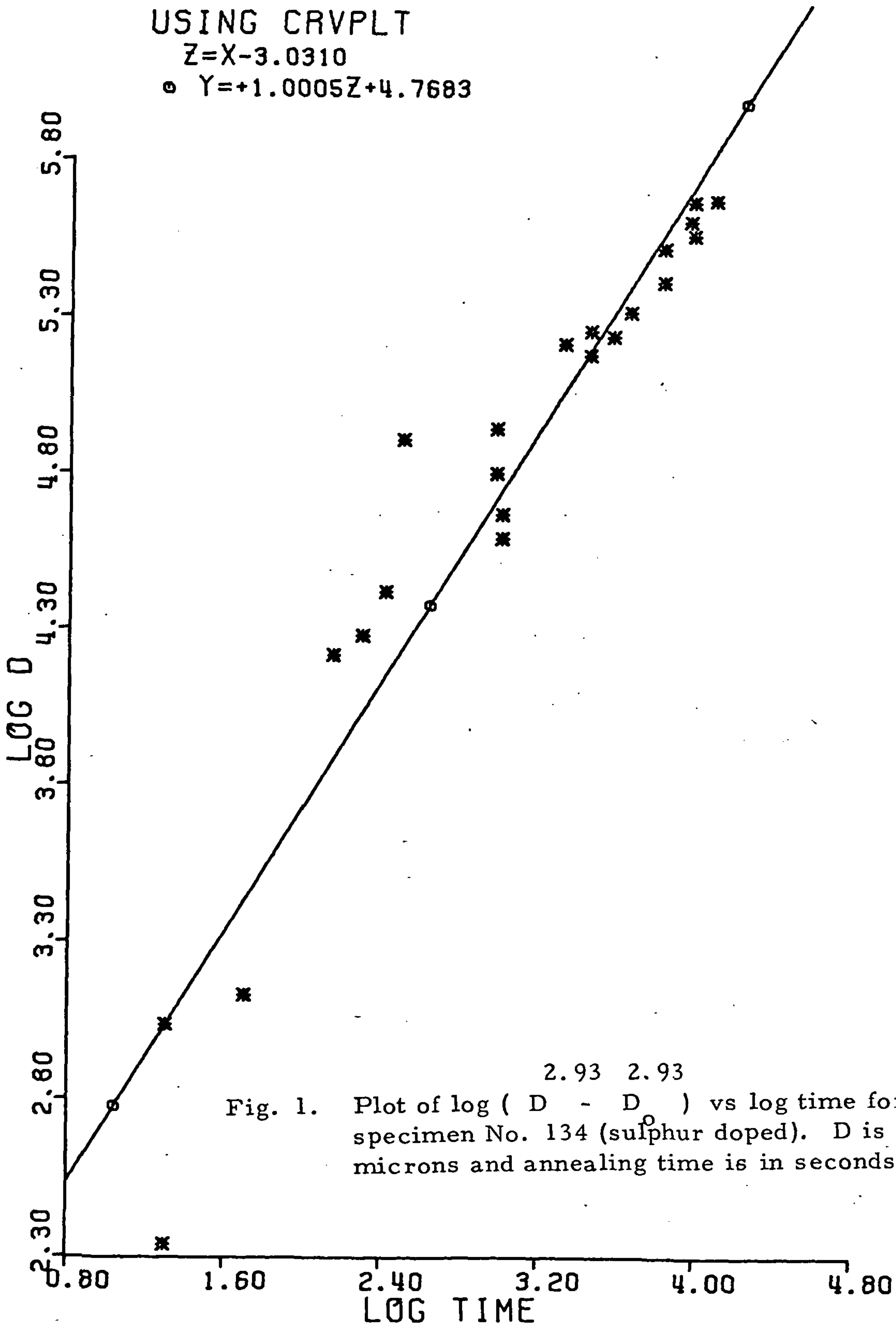

Fig. 1. Plot of log ($D^{2.93} - D_o^{2.93}$) vs log time for specimen No. 134 (sulphur doped). D is in microns and annealing time is in seconds.

Fig. 2a. Transmission electron micrograph of replicated surface of 3% flourine doped MgO. (as pressed). Polished and etched

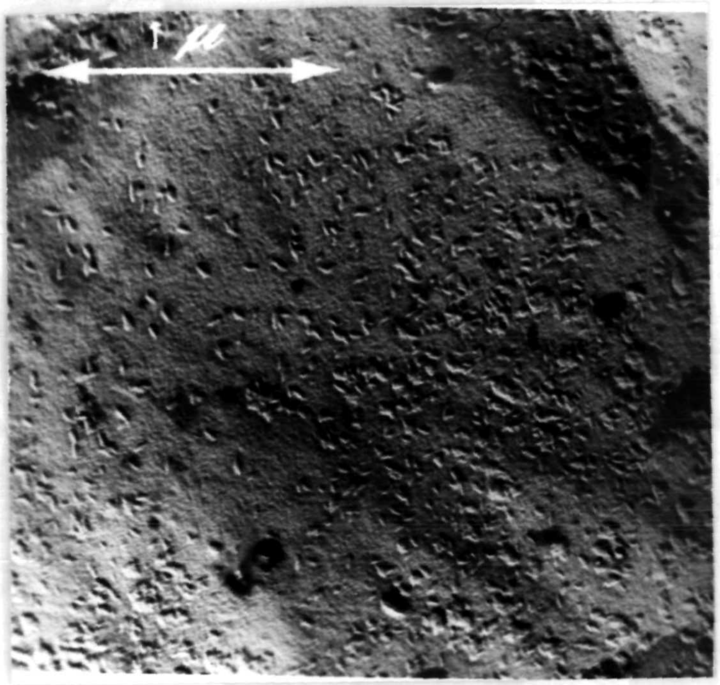

Fig. 2b. Same surface at higher magnification showing tiny platelets.

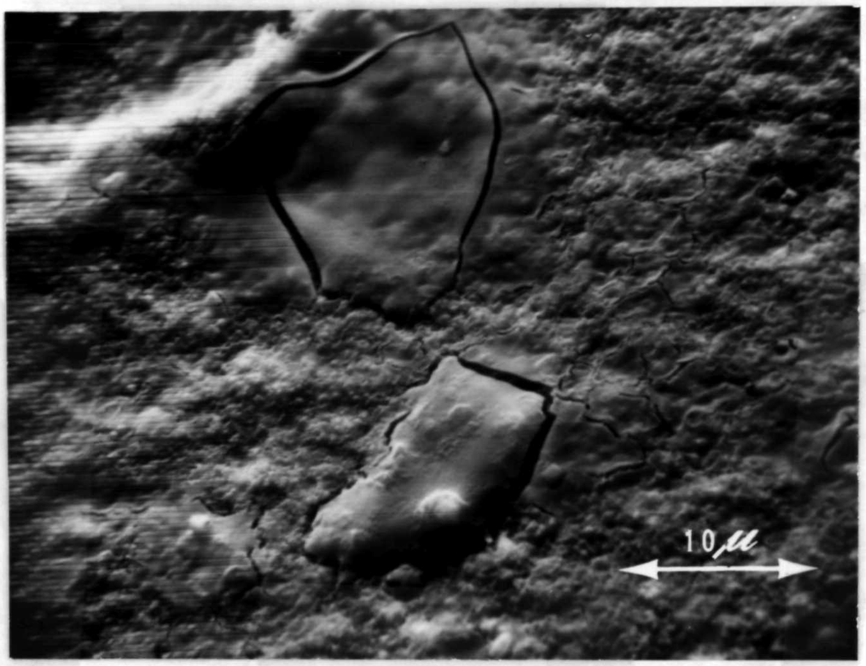

Fig. 3a. Scanning electron fractrograph (back scattered electrons, BSE) of 1.08% sulphur doped MgO (as pressed).

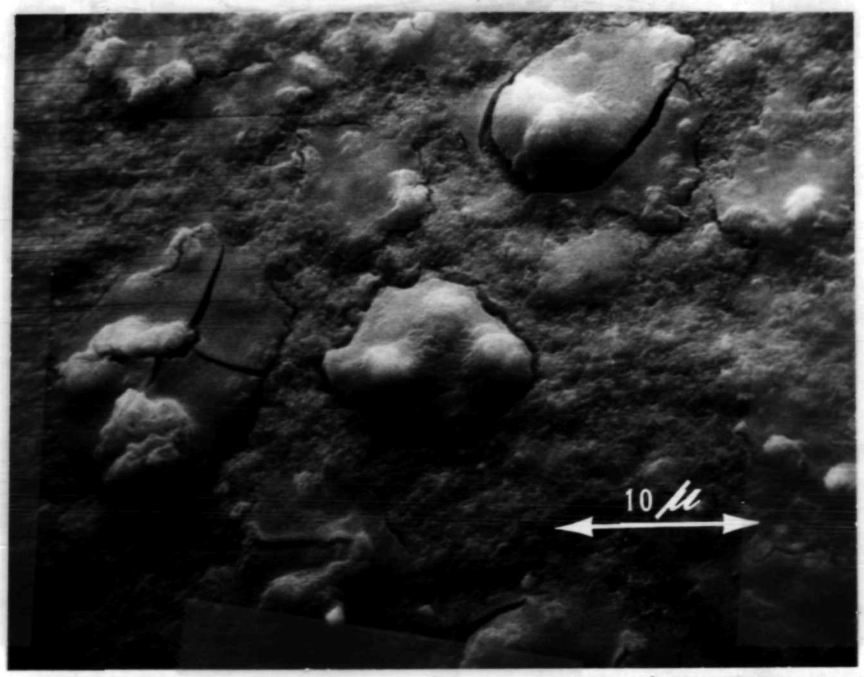

Fib. 3 b. Scanning electron fractrograph (BSE) of same sample as above but showing a different region.

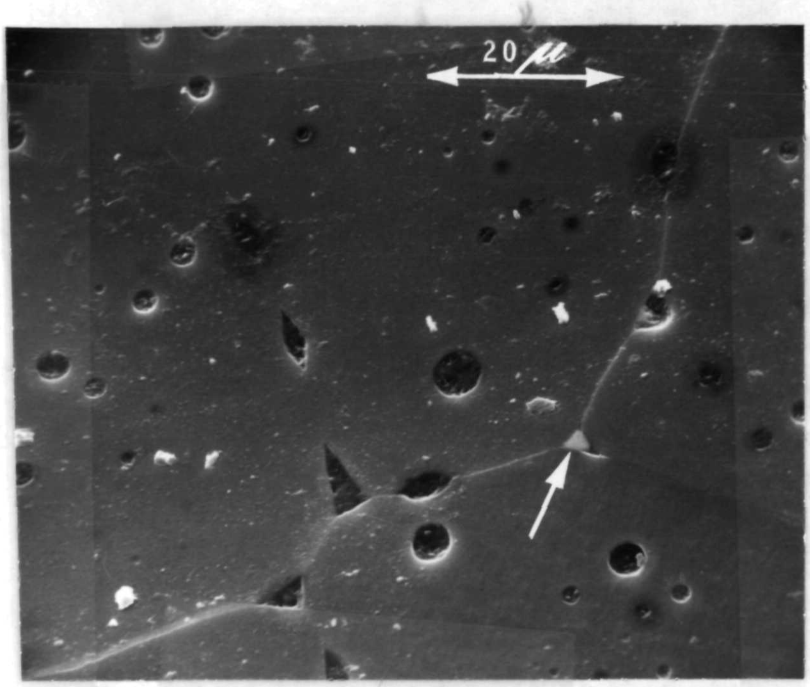

Fig. 4a. Scanning electron micrograph (BSE) of 1.08% sulphur doped MgO (reheated for 48 hours at 1500°C) Polished and etched. Arrow shows possible $CaSiO_3$ phase at triple point.

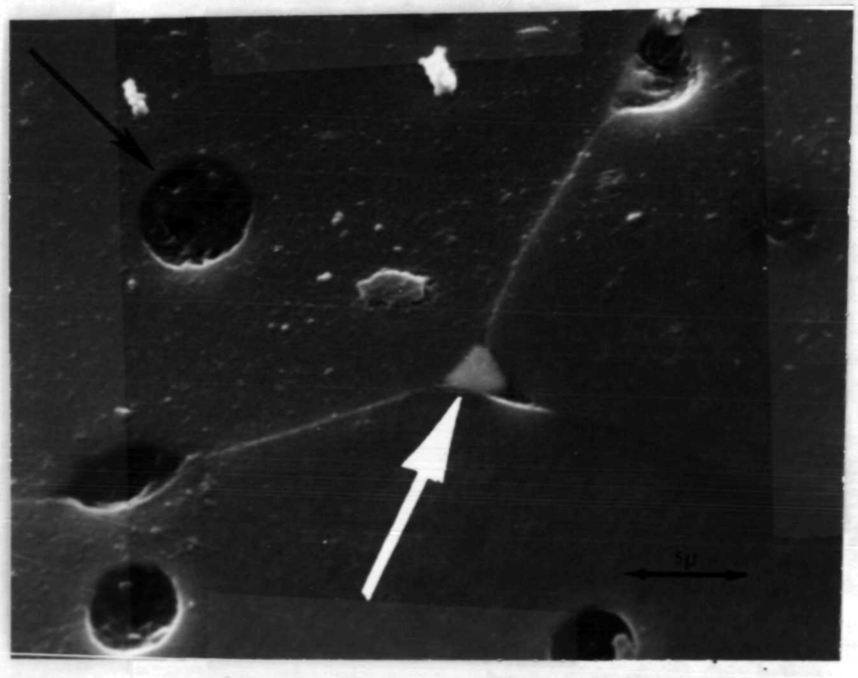

Fig. 4b. Same region as above at higher magnification indicating possible existence of second phase particles in the pore-like inclusions. Arrow (black) shows a tiny pore within one of these particles.

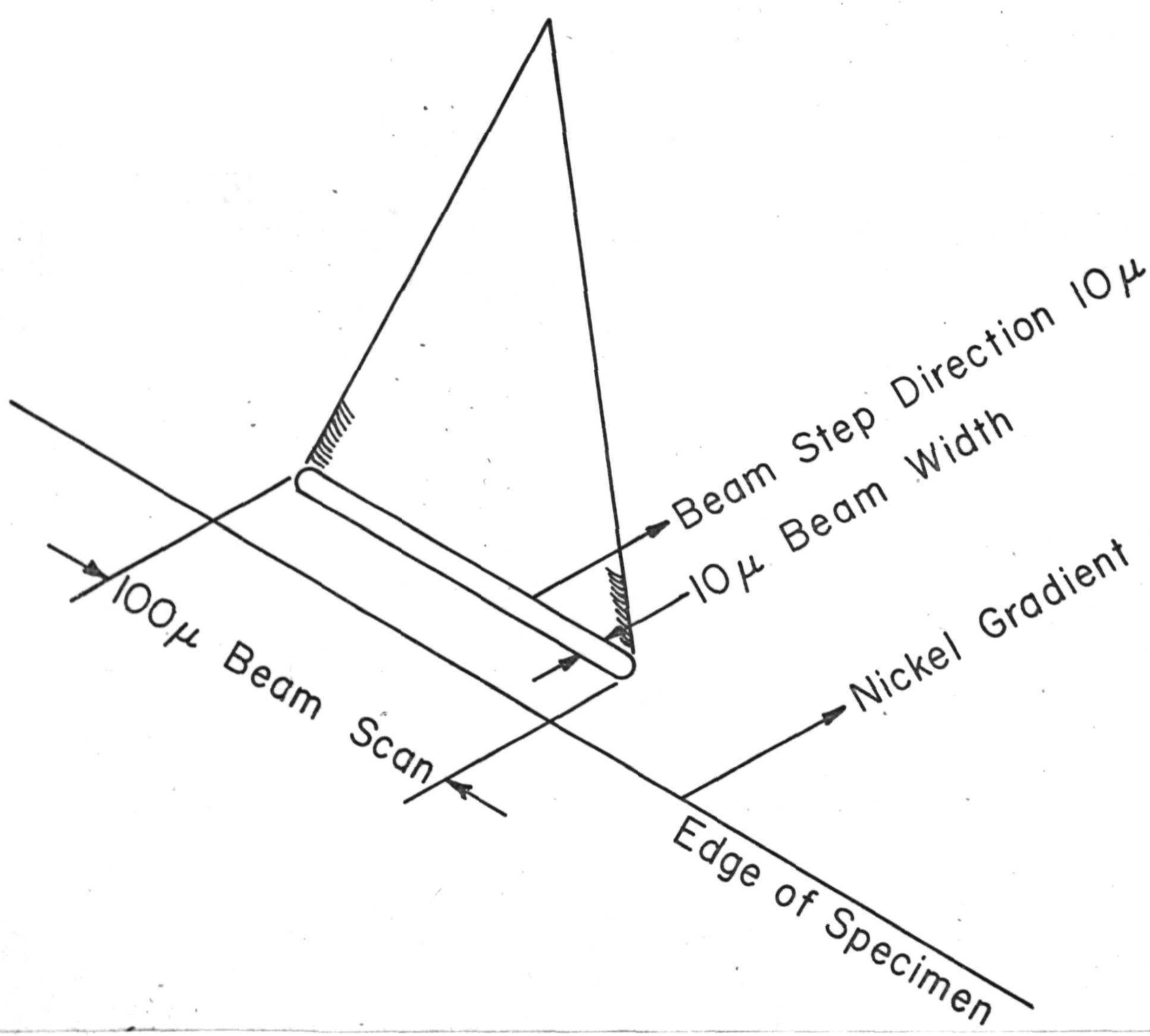

Fig. 5. Technique for determining nickel profile over extended region using electron beam microprobe.

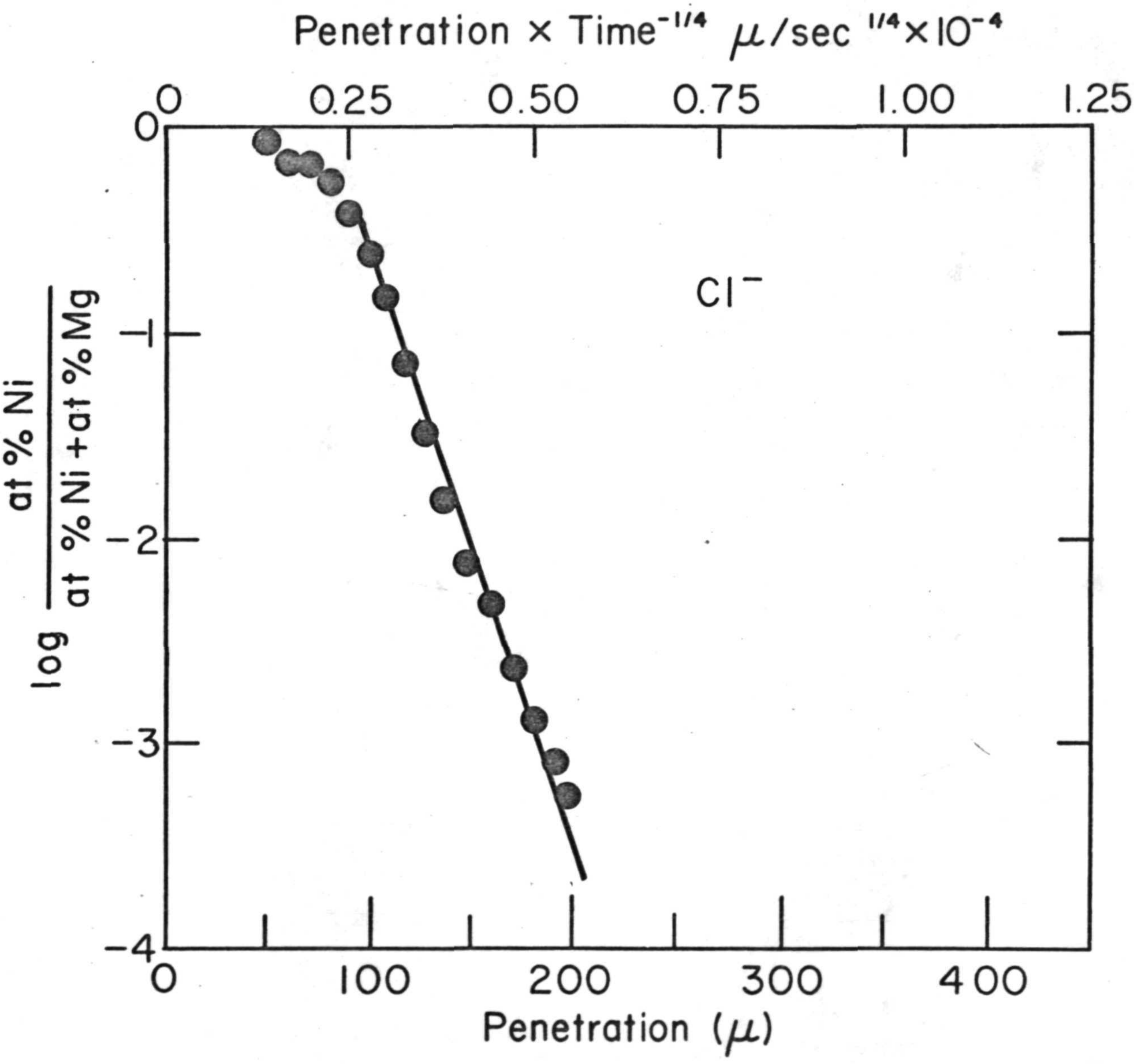

Fig. 6. Nickel fraction as a function of penetration for Cl^- doped MgO, sample 115 (1). Anneal time = 170 hrs.

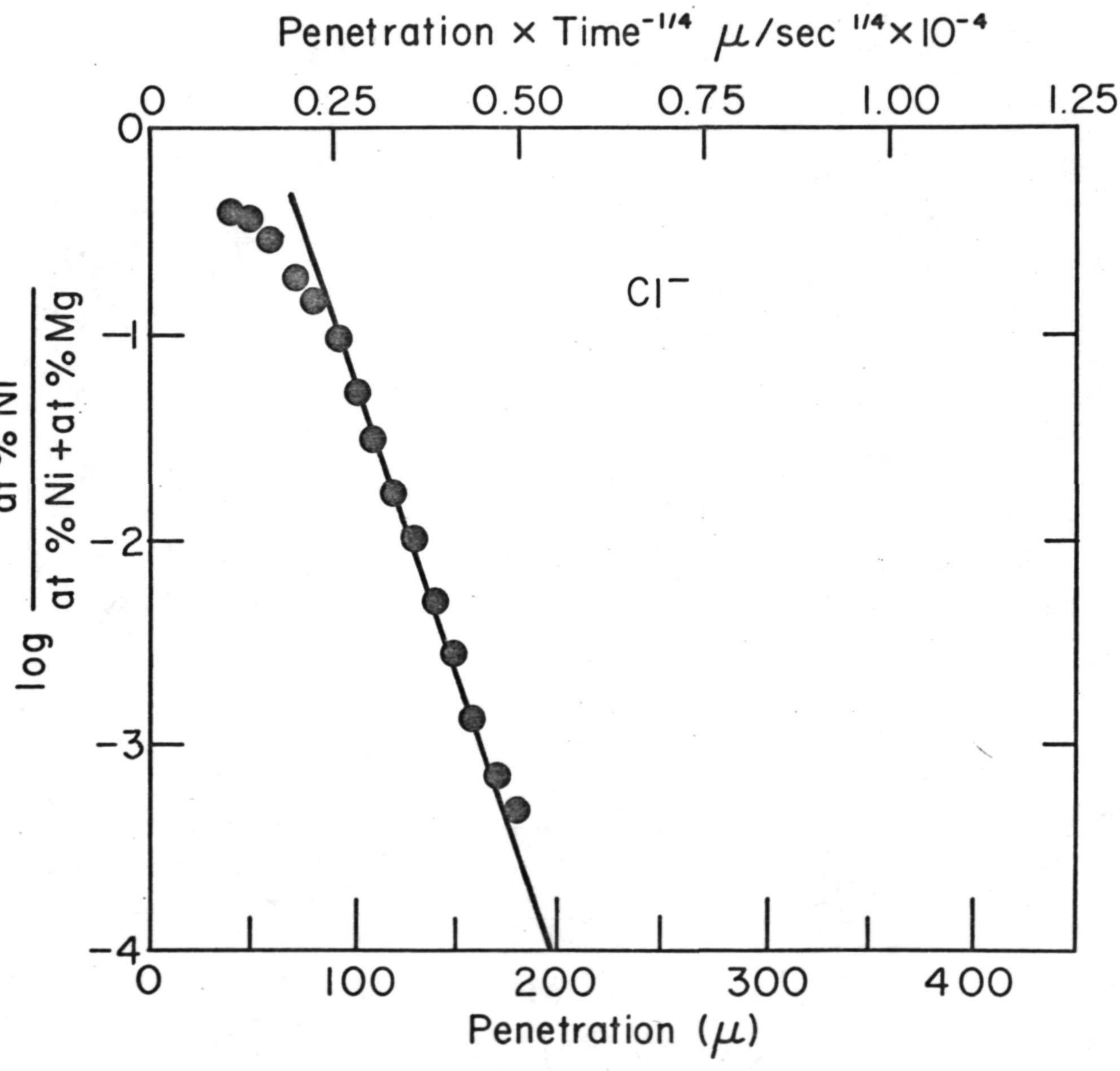

Fig. 7. Nickel fraction as a function of penetration for Cl^- doped MgO, sample 115 (2). Anneal time = 170 hrs.

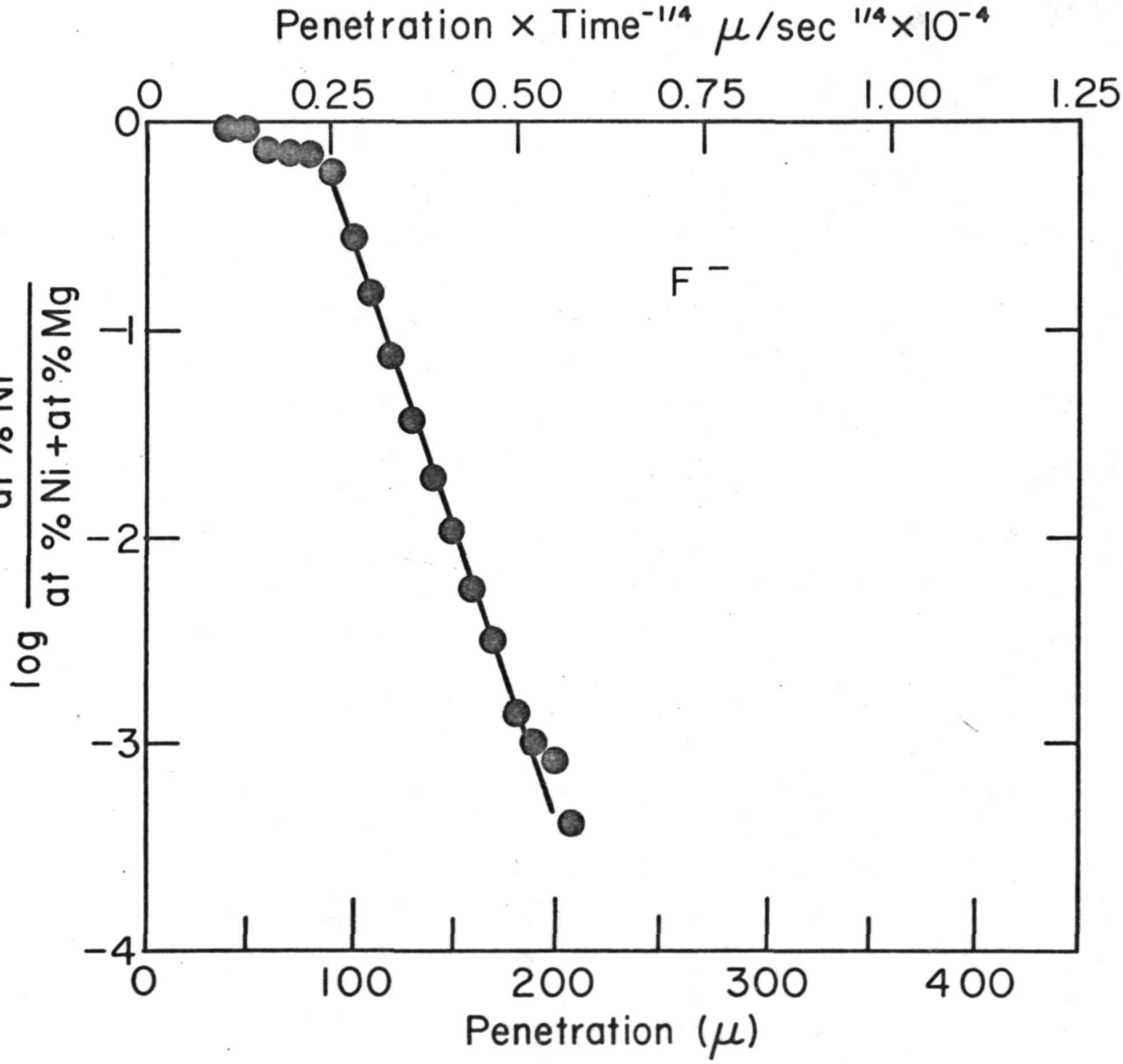

Fig. 8. Nickel fraction as a function of penetration for F^- doped MgO, sample 110. Anneal time = 170 hrs.

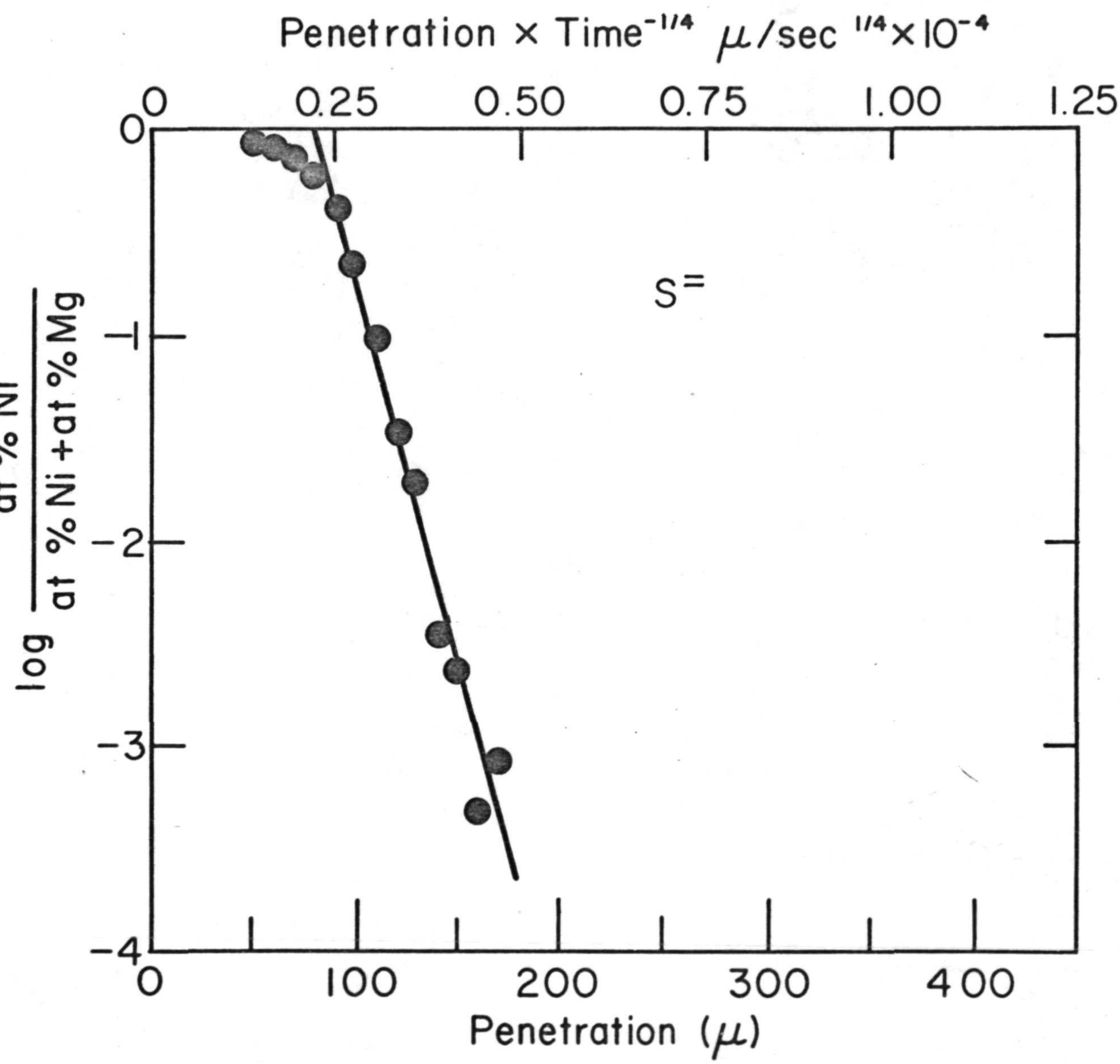

Fig. 9. Nickel fraction as a function of penetration for $S^{=}$ doped MgO, sample 30. Anneal time = 170 hrs.

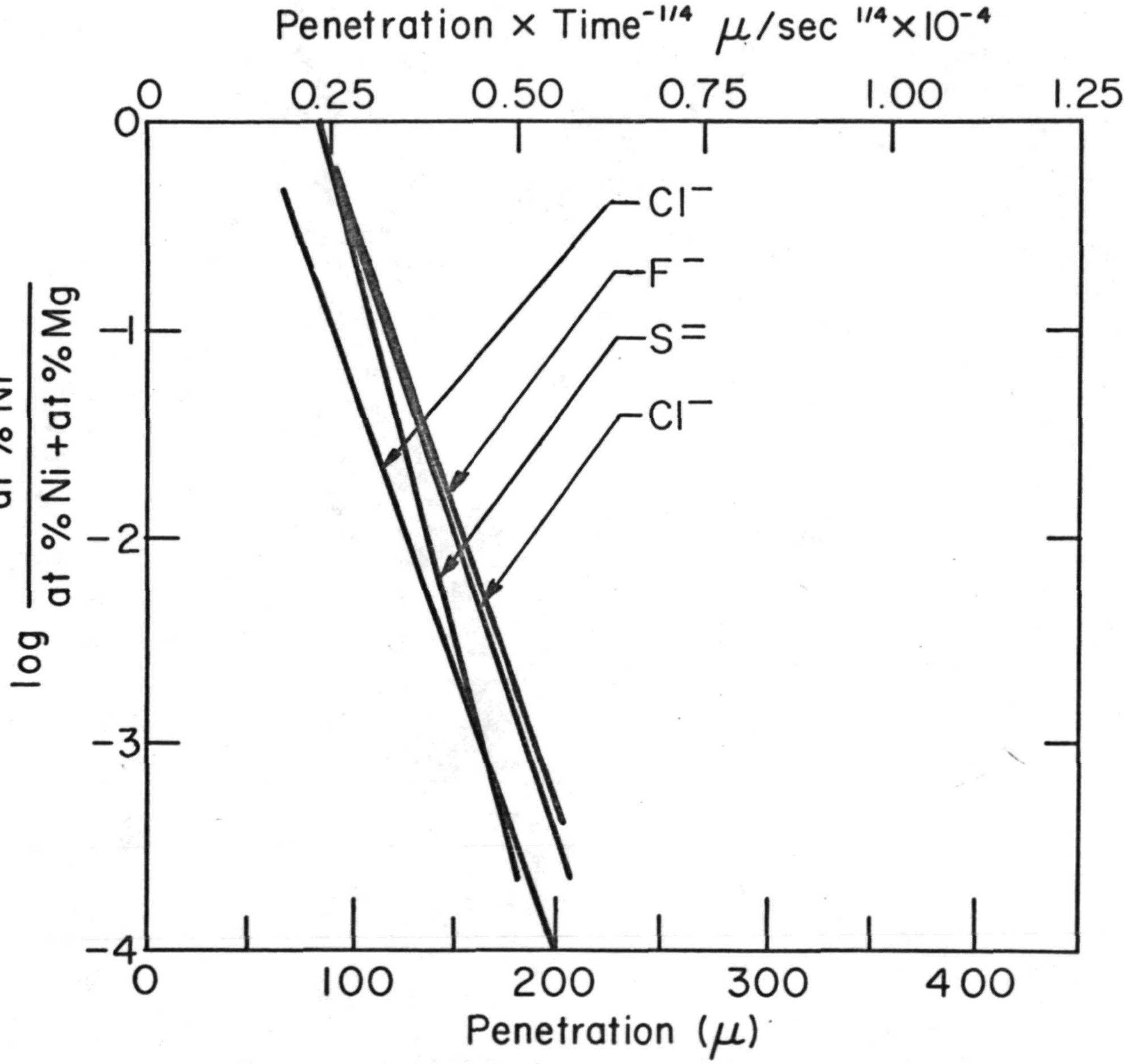

Fig. 10. Composite nickel fraction as a function of penetration for various dopants. Anneal time = 170 hrs.

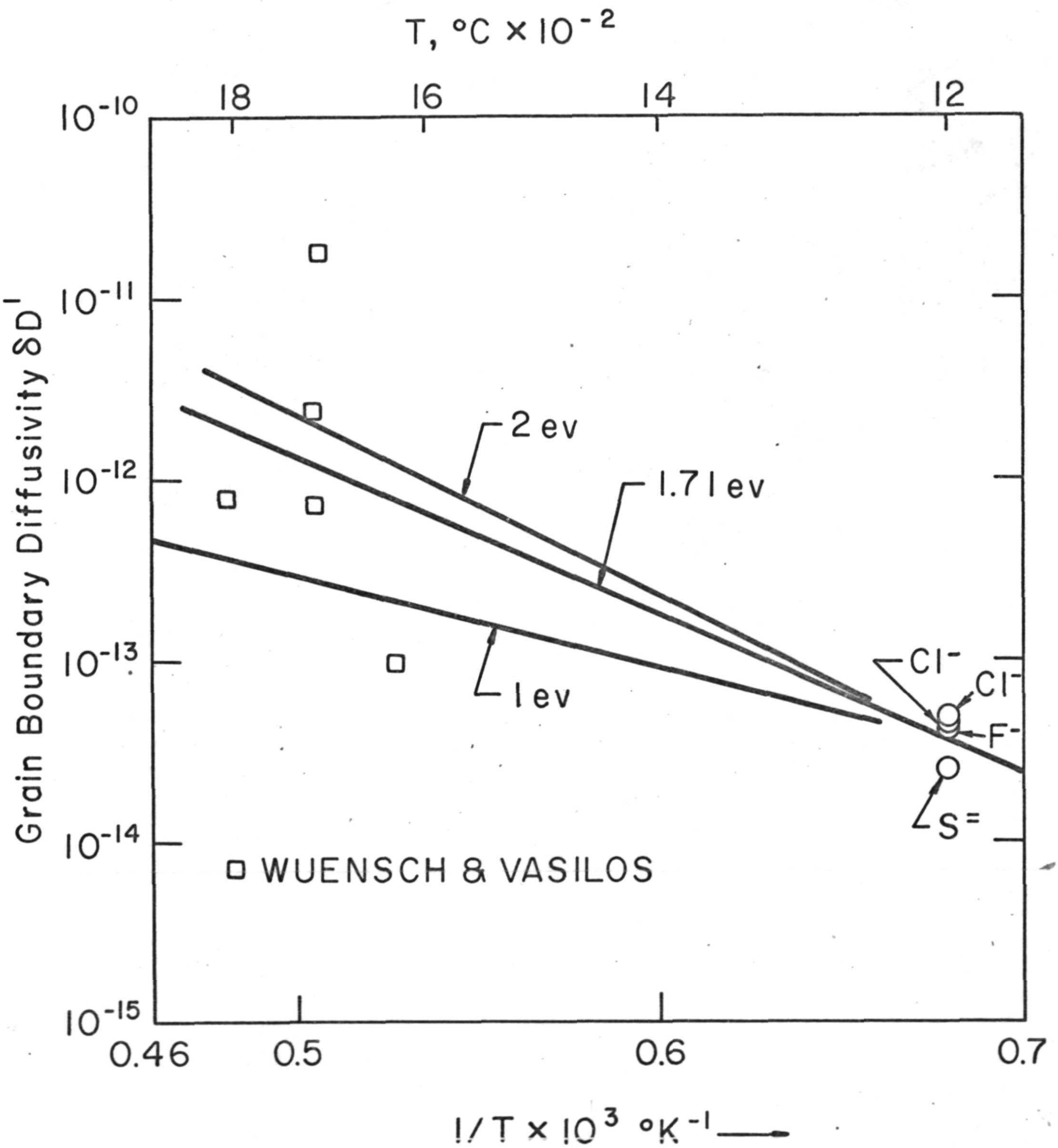

Fig. 11. Diffusivity of Ni in polycrystalline MgO as a function of temperature, anion-doped from this work.

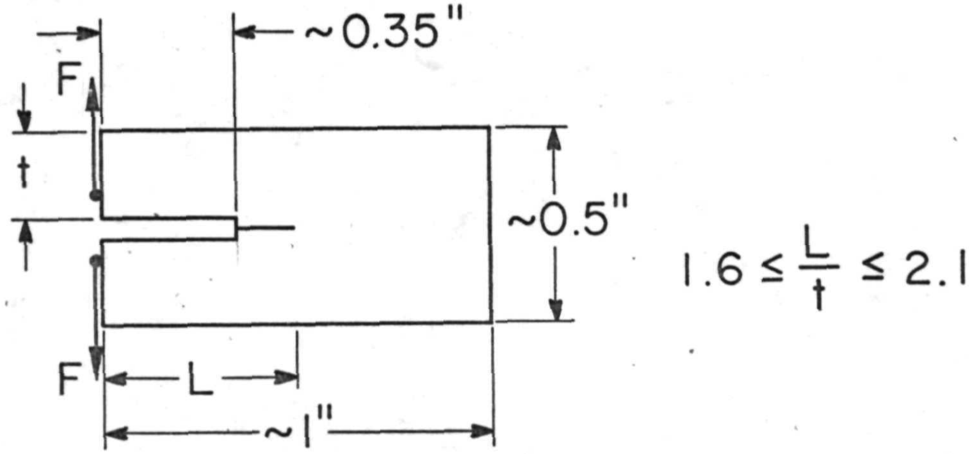

Fig 12. Double Cantilever Beam fracture toughness specimen configuration.

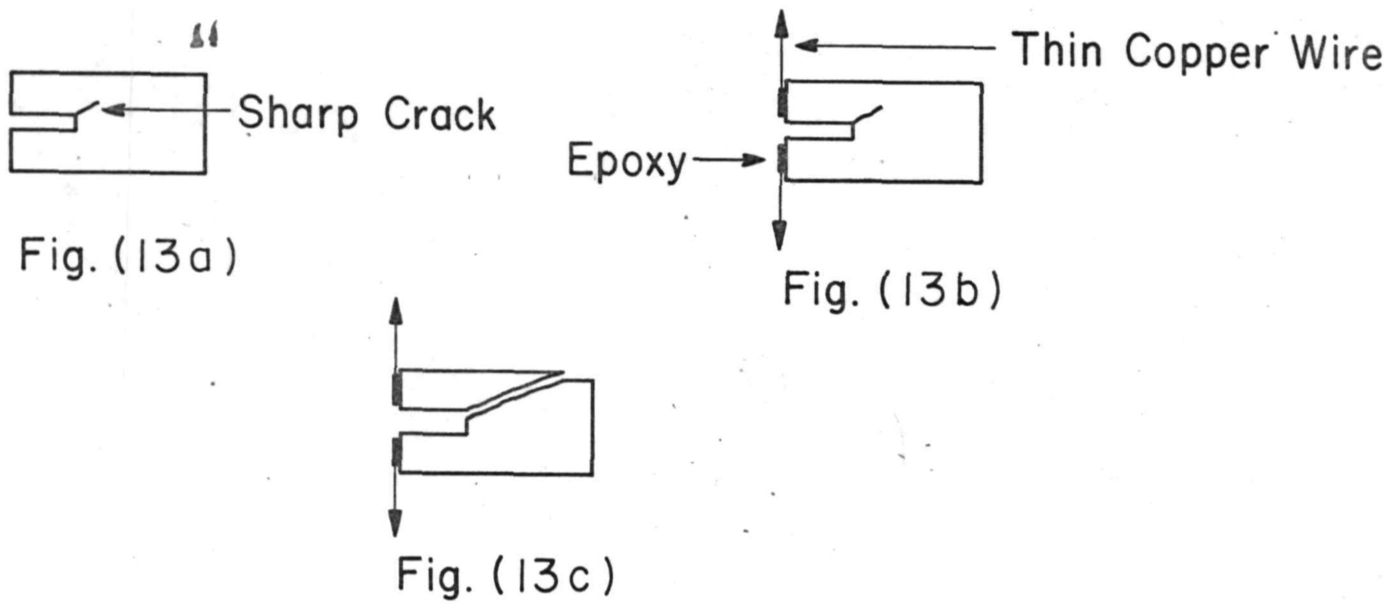

Fig. 13. Various fracture toughness specimens showing crack configuration method of attachment and typical failure.

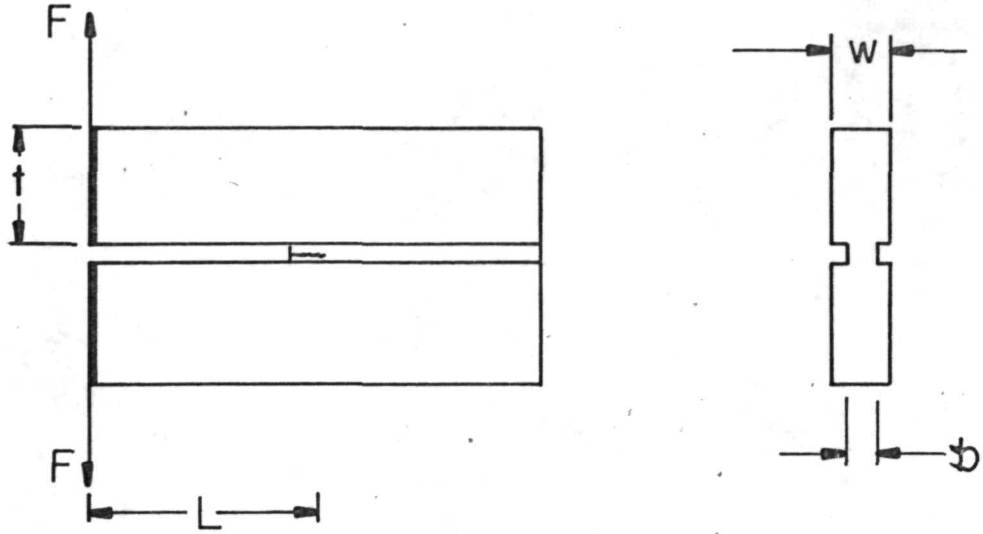

Fig. 14. Double Cantilever Specimen with a groove

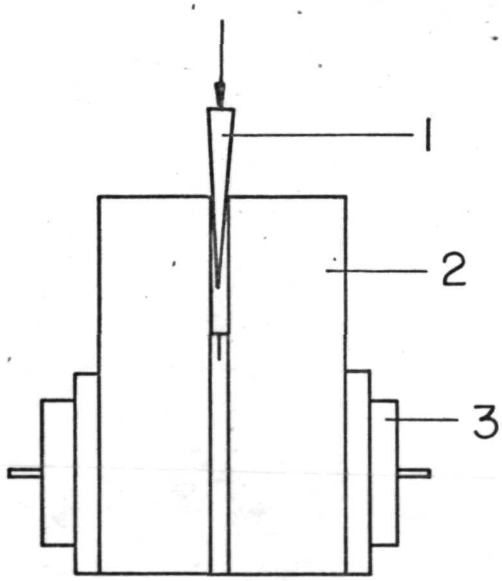

Fig. 15. Wedge technique of producing a sharp crack.
1 Wedge
2 Specimen
3 Clamps

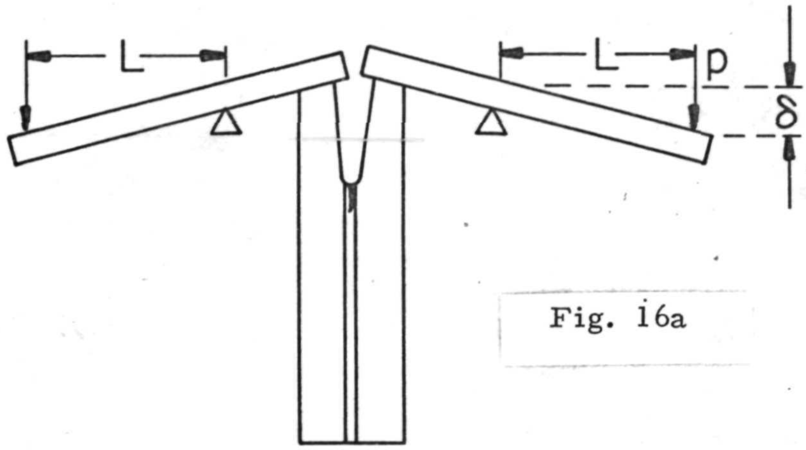

Fig. 16a

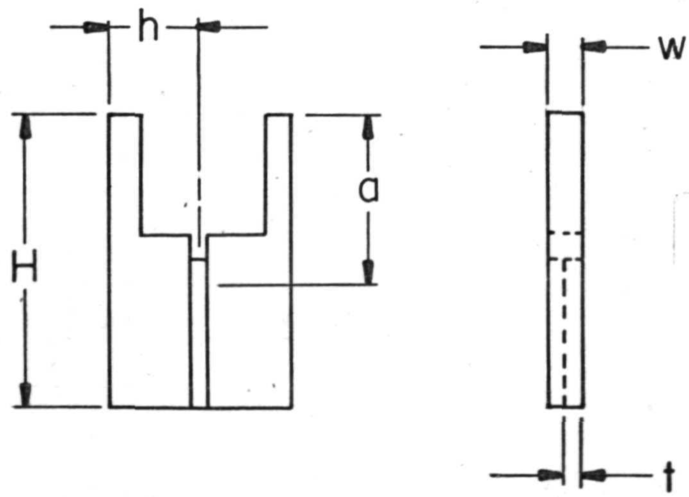

Fig. 16b

Fig. 16. a. Schematic view of constant moment beam technique (ref.16).

b. Specimen design used in this research

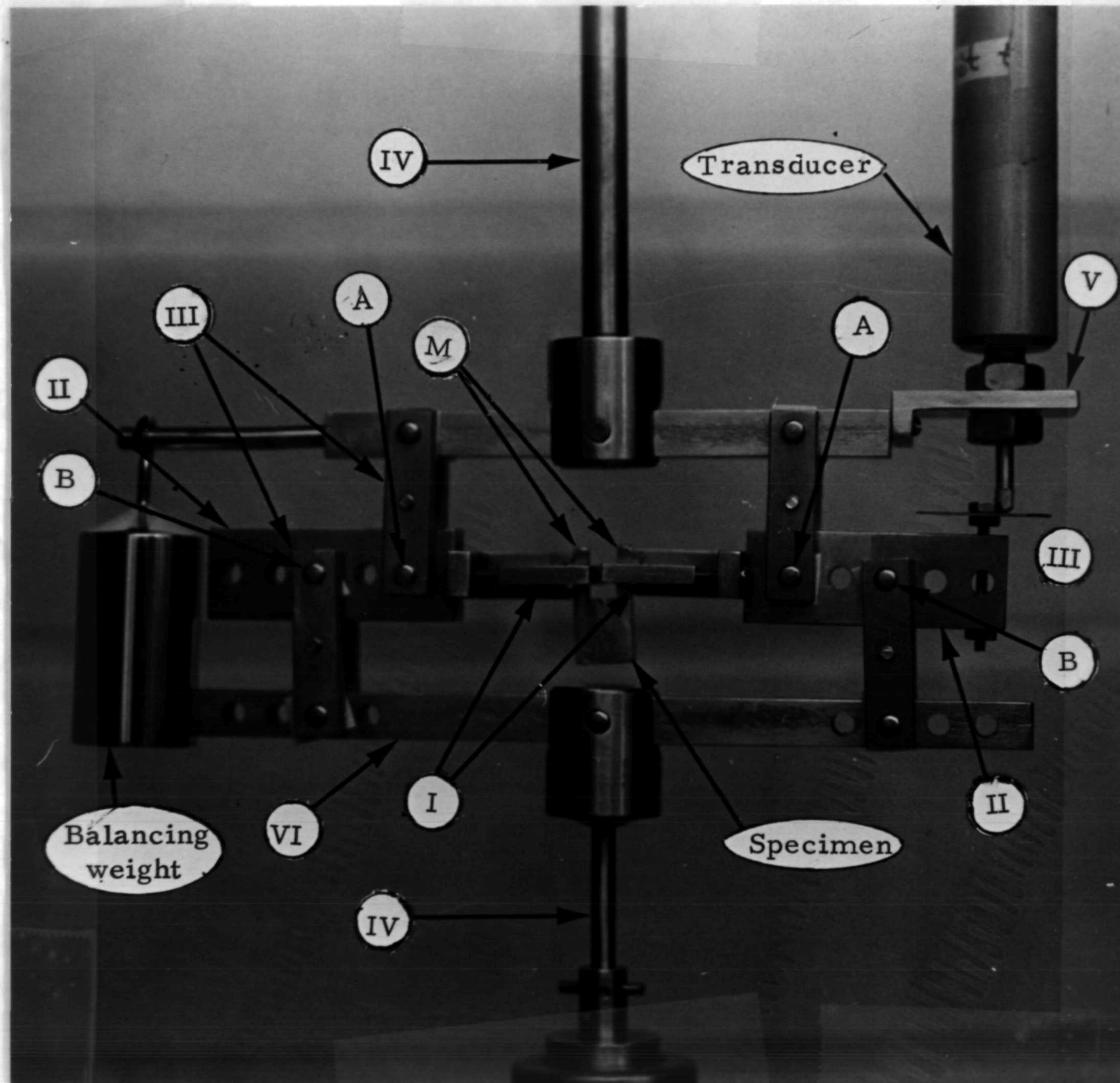

Fig. 17. Present Test Device for Constant Moment Beam Testing.

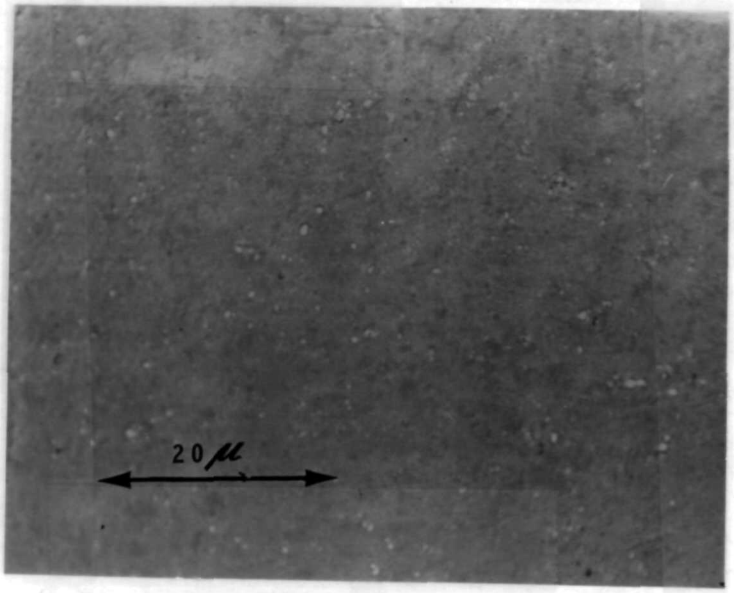

Fig. 18. Si_3N_4 polished specimen.
Material Norton HS-130

Fig. 19. Si_3N_4 polished specimen treated with phosphoric acid at 200°C for 45 hrs. but not treated with HF. Material Norton HS-130.

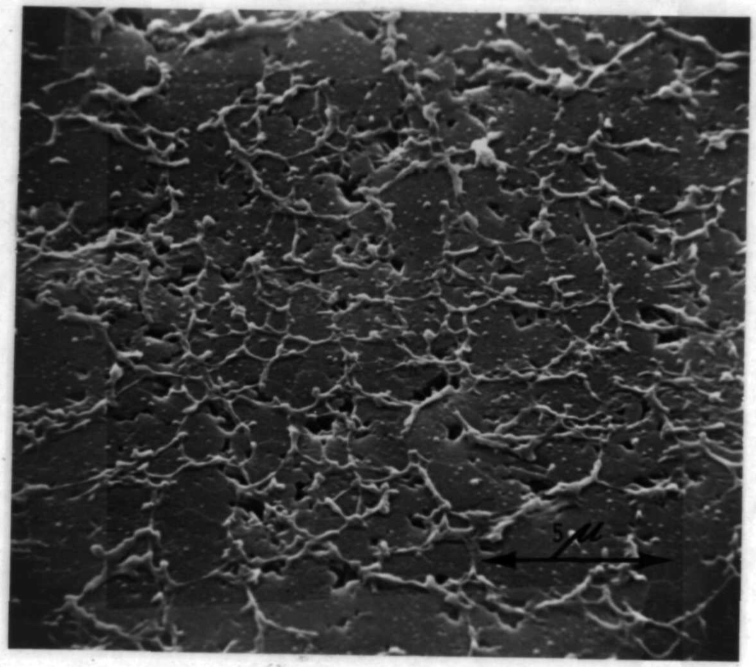

Fig. 20. Si_3N_4 polished specimen treated with boiling H_3PO_4 at 200°C for 20 hrs. and then kept in HF for 2 hrs. Material Norton HS-130